IEEE Access
Multidisciplinary | Rapid Review | Open Access Journal

Received December 24, 2018, accepted January 21, 2019, date of publication January 25, 2019, date of current version February 12, 2019.

Digital Object Identifier 10.1109/ACCESS.2019.2895512

Robust Model-Free Nonsingular Terminal Sliding Mode Control for PMSM Demagnetization Fault

KAIHUI ZHAO, TONGHUAN YIN, CHANGFAN ZHANG, JING HE, XIANGFEI LI, YUE CHEN, RUIRUI ZHOU, AND AOJIE LENG

College of Electrical and Information Engineering, Hunan University of Technology, Zhuzhou 412007, China

Corresponding author: Jing He (hejing@263.net)

This work was supported in part by the National Key Research and Development Program of China under Grant 2018YFD0400705, in part by the Natural Science Foundation of China under Grant 61473117, Grant 61773159, and Grant 61503131, in part by the Hunan Provincial Natural Science Foundation of China under Grant 2018JJ2093, Grant 2018JJ4066, Grant 2017JJ4031, and Grant 2016JJ5012, in part by the Scientific Research Fund of the Hunan Provincial Education Department under Grant 16A058 and Grant 17B073, and in part by the Key Laboratory for Electric Drive Control and Intelligent Equipment of Hunan Province under Grant 2016TP1018.

ABSTRACT In this paper, a robust model-free nonsingular terminal sliding-mode control (MFNTSMC) algorithm based on the ultra-local model is proposed to reduce the influence of permanent magnet (PM) demagnetization for PM synchronous motors (PMSMs). First, the PMSM mathematical model in normal and demagnetization is described, and the ultra-local model of speed loop and current loop is constructed based on the input and the output of the PMSM vector control system. Then, the MFNTSMC method is proposed and adopted to design the speed controller and *d*-*q*-axis current controller, and the sliding-mode observer is designed to estimate the unknown terms of the ultra-local model. Finally, compared with the PI control method and model-free control method, the results of simulations and experimentations show that the MFNTSMC method can improve the dynamic response while maintaining robustness of PMSM driven system, reduce the dependence of the design of controller on the precise PMSM model, and has fault-tolerant control function for PM demagnetization fault.

INDEX TERMS Ultra-local model, permanent magnet synchronous motor (PMSM), demagnetization, model-free nonsingular terminal sliding mode control (MFNTSMC), sliding mode observer (SMO).

I. INTRODUCTION

Permanent magnet synchronous motors (PMSMs) have gradually become one of the most potential motors in industry field due to its advantages of simple structure, high efficiency and energy saving [1]. In recent years, PMSMs have been widely applied in railway traction system, electric vehicle, aerospace and other fields. The traditional proportional-integral (PI) control scheme are widely applied in the speed controller and current controller of PMSM drive systems, because of their simplicity and easy implementation. However, traditional PI controller is difficult to meet the control requirements of high-performance drive systems because of integral windup [2].

The stability of permanent magnets (PM) is often affected by temperature, electromagnetic field and other factors, in severe cases even leading to the demagnetization fault. The demagnetization has direct influence on the accuracy PMSM drive system [3], [4]. In [5], the terminal sliding mode controller based on nonlinear disturbance observer is designed to overcome the effect of the parameter perturbation. In [6], a robust fault-tolerant predictive current control method is proposed for PMSM considering demagnetization fault, and the fault tolerance and robustness are verified by simulation and experimental results. In [7], a fault-tolerant predictive control algorithm based on active flux linkage is proposed, the SMO is designed to estimate active flux linkage; deadbeat control strategy is adopted to eliminate the error of active flux linkage. The proposed methods in [5]–[7] are all model-based control methods, while the model of PMSM is uncertain when parameter perturbation is considered.

Compared with model-based control methods, the model-free control (MFC) method can reduce the dependence on the system model, and significantly improve the control performance of motor [8], [9]. The MFC is appropriate for nonlinear, uncertain, strongly coupled PMSM driven systems.

The associate editor coordinating the review of this manuscript and approving it for publication was Bora Onat.

The MFC is proposed based on the ultra-local model, which is established with the input and output of the system [10]–[12]. In [13], the model-free controller is designed to control a two-tank system, and the experimental results show that the MFC method has the merit of robustness and simple implementation. In [14], aiming at the robust synchronization problem of master slave chaotic systems, the ultra-local model is established, and the fixed-time differentiator is used to estimate the unmeasurable states. In [15], the predictive current controller of PMSM is designed based on ultra-local model. The method has faster transient performance and smaller pulsation. In [16], aiming at the problem that the parametric uncertainties and inverter nonlinearity in PMSM, a model-free deadbeat predictive current control (MFDPCC) method is proposed. Compared with conventional PI controller and model-based deadbeat predictive current controller, MFDPCC has stronger robustness.

In this paper, a model-free nonsingular terminal sliding mode control (MFNTSMC) method is proposed, which combines model-free control [10], [17] with nonsingular terminal sliding mode control (NTSMC) [18], to guarantee reliable operation of PMSM regardless of PM demagnetization fault and external disturbances. The ultra-local model based on the input and output of PMSM is established, to reduce the dependence of the controller on the precise PMSM model. The speed and current controllers are designed by MFNTSMC algorithm, so as to improve the response speed and steady state tracking accuracy of the PMSM system, and the SMO is designed to estimate the unknown variable of the ultra-local model. The results of simulations and experimentations show that the proposed method has faster response speed and higher control accuracy, and has fault-tolerant control function for PM demagnetization fault.

The remainder of this paper is organized as follows. The mathematical model of PMSM in normal and demagnetization is described, and the ultra-local model of PMSM is established in Section II. A MFNTSMC controller and a SMO are designed in Section III. The results of simulation and experimental are shown in Section IV and V. A brief conclusion is presented in Section VI.

II. SYSTEM DESCRIPTION

A. MATHEMATICAL MODEL OF PMSM IN NORMAL CONDITION

The stator voltage equations of the healthy PMSM in the d-q-axis reference frame can be expressed as follows [18]:

$$\begin{cases} u_d = R_s i_d + \dfrac{d\psi_d}{dt} - \omega_e \psi_q \\ u_q = R_s i_q + \dfrac{d\psi_q}{dt} + \omega_e \psi_d, \end{cases} \tag{1}$$

where u_d, u_q are the d- and q-axis voltage (V), respectively; i_d, i_q are the d- and q-axis stator currents (A), respectively; ψ_d, ψ_q are the d- and q-axis stator flux linkage (Wb), respectively; R_s is stator resistance (Ω), and ω_e is the rotor electrical angular velocity (rad/s).

The stator flux linkage of PMSM is expressed as follows:

$$\begin{cases} \psi_d = L_d i_d + \psi_{ro} \\ \psi_q = L_q i_q, \end{cases} \tag{2}$$

where L_d, L_q are the d- and q-axis stator inductances (H), respectively; ψ_{ro} is the normal parameters of the rotor PM flux linkage (Wb).

The electromagnetic torque equation of PMSM in the d-q-axis reference frame can be expressed as:

$$\begin{aligned} T_e &= \frac{3}{2} n_p \left(\psi_d i_q - \psi_q i_d \right) \\ &= \frac{3}{2} n_p \left[\psi_{ro} + \left(L_d - L_q \right) i_d \right] i_q \\ &= \frac{3}{2} n_p \psi_{ext} i_q, \end{aligned} \tag{3}$$

where T_e is the electromagnetic torque(Nm); n_p is the number of pole pairs; ψ_{ext} represents the active flux [19]–[21].

The speed equation of PMSM in the d-q-axis reference frame is as follows:

$$\frac{d\omega_e}{dt} = \frac{n_p}{J} \left(T_e - T_L - B\omega_m \right), \tag{4}$$

where T_L is the load torque(Nm); ω_m is the rotor mechanical angular velocity (rad/s), and $\omega_e = n_p \omega_m$; J is the moment of inertia (kg·m^2); B is the viscous friction coefficient (Nm·s/rad), and $B\omega_m$ is the viscous friction torque.

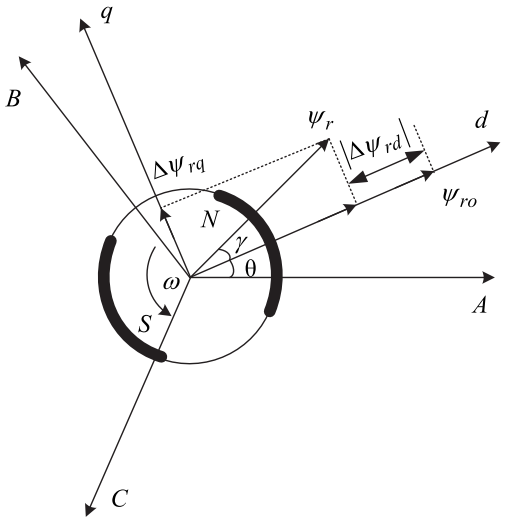

FIGURE 1. Variation of PMSM flux-linkage.

B. MATHEMATICAL MODEL OF PMSM WITH PM DEMAGNETIZATION

The permanent magnet (PM) demagnetization occurs because of the external influence, such as temperature rise and other external factors [22]. When the PM demagnetization fault occurs, the PM flux linkage amplitude and direction will change. The flux linkage amplitude varies from initial ψ_{ro} to ψ_r, and a deviation angle γ exists between the direction of the rotor flux and the d-axis of the reference frame. It is illustrated in Figure 1 [2], [22].

When the PM demagnetization fault occurs, the equation (2) no longer holds, and stator flux-linkage of PMSM are formed as follows:

$$\begin{cases} \psi_d = \psi_{ro} + L_d i_d + \Delta\psi_{rd} \\ \psi_q = L_q i_q + \Delta\psi_{rq}, \end{cases} \tag{5}$$

where $\Delta\psi_{rd}$ is perturbation values of the flux-linkage components of d-axis, $\Delta\psi_{rd} = \psi_r \cos\gamma - \psi_{ro}$; $\Delta\psi_{rq}$ is perturbation values of the flux linkage components of q-axis, $\Delta\psi_{rq} = \psi_r \sin\gamma$; $\gamma \in \left[0, \frac{\pi}{2}\right)$.

Substituting (5) into (1), the stator voltage equations of PMSM is expressed as follows when PM demagnetization fault occurs:

$$\begin{cases} u_d = R_s i_d - \omega_e L_q i_q + L_d \dfrac{di_d}{dt} \\ \qquad + \dfrac{d(\psi_{ro} + \Delta\psi_{rd})}{dt} - \omega_e \Delta\psi_{rq} \\ u_q = R_s i_q + \omega_e L_d i_d + L_q \dfrac{di_q}{dt} + \dfrac{d\Delta\psi_{rq}}{dt} \\ \qquad + \omega_e(\psi_{ro} + \Delta\psi_{rd}). \end{cases} \tag{6}$$

Considering that the time constant of the mechanical system is much larger than that of the electrical system in the PMSM, that is $\frac{d(\psi_{ro}+\Delta\psi_{rd})}{dt} \approx 0$, $\frac{d\Delta\psi_{rq}}{dt} \approx 0$ [2]. Then, the stator voltage (6) of PMSM can be rearranged as follows:

$$\begin{cases} u_d = R_s i_d - \omega_e L_q i_q + L_d \dfrac{di_d}{dt} - \omega_e \Delta\psi_{rq} \\ u_q = R_s i_q + \omega_e L_d i_d + L_q \dfrac{di_q}{dt} + \omega_e(\psi_{ro} + \Delta\psi_{rd}). \end{cases} \tag{7}$$

According to (7), the state equations of PMSM in d-q-axis reference frame can be expressed as follows:

$$\begin{cases} \dfrac{di_d}{dt} = \dfrac{u_d}{L_d} - \dfrac{R_s}{L_d} i_d + \omega_e \dfrac{L_q}{L_d} i_q + \omega_e \dfrac{\Delta\psi_{rq}}{L_d} \\ \dfrac{di_q}{dt} = \dfrac{u_q}{L_q} - \dfrac{R_s}{L_q} i_q - \omega_e \dfrac{L_d}{L_q} i_d - \omega_e \dfrac{\psi_{ro} + \Delta\psi_{rd}}{L_q}. \end{cases} \tag{8}$$

The electromagnetic torque (3) of PMSM can be rearranged as follows:

$$\begin{aligned} T_e &= \frac{3}{2} n_p \left(\psi_d i_q - \psi_q i_d\right) \\ &= \frac{3}{2} n_p \left[\left(\psi_{ro} + \left(L_d - L_q\right) i_d\right) i_q + \Delta\psi_{rd} i_q - \Delta\psi_{rq} i_d\right] \\ &= \frac{3}{2} n_p \psi_{ext} i_q + \frac{3}{2} n_p \left(\Delta\psi_{rd} i_q - \Delta\psi_{rq} i_d\right). \end{aligned} \tag{9}$$

According to (4) and (9), the speed equation can be rearranged as follows when PM demagnetization fault are considered:

$$\begin{aligned} &\frac{d\omega_e}{dt} \\ &= \frac{n_p}{J}\left[\frac{3}{2} n_p \left(\psi_{ext} i_q + \left(\Delta\psi_{rd} i_q - \Delta\psi_{rq} i_d\right)\right) - T_L - B\omega_m\right] \\ &= \frac{3n_p^2}{2J} \psi_{ro} i_q + \frac{3n_p^2}{2J} \left(L_d - L_q\right) i_d i_q \\ &\quad + \frac{3n_p^2}{2J} \left(\Delta\psi_{rd} i_q - \Delta\psi_{rq} i_d\right) - \frac{n_p}{J} \left(T_L + B\omega_m\right). \end{aligned} \tag{10}$$

C. THE ULTRA-LOCAL MODEL OF PMSM

According to input and output of the system, some nonlinear, complex and variable systems can be replaced by ultra-local model. A first-order ultra-local model of a single-input and single-output system is expressed as follows [10]:

$$\frac{dy}{dt} = \alpha u + F, \tag{11}$$

where y and u are the output and control variables of system; α is a non-physical constant parameter; F denotes known parts of the system and unmodeled dynamics.

In order to reduce the dependence of the speed controller and current controller on the PMSM system model, and the influence of the PM demagnetization fault on the controller, according to (8) and (10), the ultra-local model of the speed loop and current loop for PMSM can be designed as follows:

$$\begin{cases} \dfrac{di_d}{dt} = \alpha_d u_d + F_d \\ \dfrac{di_q}{dt} = \alpha_q u_q + F_q \\ \dfrac{d\omega_e}{dt} = \alpha_\omega i_q + F_\omega, \end{cases} \tag{12}$$

where α_d, α_q are the designed voltage parameter, α_ω is the designed current parameter; F_d, F_q, F_ω are known parts of the mathematical model of PMSM in normal condition and the PM demagnetization fault, and they are all bounded quantities.

According to ultra-local model (12), the equation can be rearranged as follows:

$$\dot{\boldsymbol{x}} = \boldsymbol{\alpha u} + \boldsymbol{F}, \tag{13}$$

where $\boldsymbol{x} = \left[i_d \ i_q \ \omega_e\right]^T$; $\boldsymbol{\alpha} = diag\left(\alpha_d, \alpha_q, \alpha_\omega\right)$; $\boldsymbol{u} = \left[u_d \ u_q \ i_q\right]^T$; $\boldsymbol{F} = \left[F_d \ F_q \ F_\omega\right]^T$.

Remark 1: The ultra-local model of PMSM is constructed. When the PM demagnetization fault occurs, the $\boldsymbol{F}$ *will change. The SMO is used to estimate the variable* $\hat{\boldsymbol{F}}$ *and feed back to the MFNTSMC controller. The MFNTSMC method can be used to design the d-q-axis current controllers and speed controller without depending on the specific model of the nonlinear PMSM system.*

III. MFNTSMC METHOD WITH SMO

In order to obtain higher steady-state tracking accuracy, reduce the dependence of the design of controller on the precise PMSM model, the MFNTSMC method is proposed in this paper.

Figure 2 illustrates the structure of MFNTSMC. The schematic diagram includes MFNCSMC controller and SMO. The SMO is used to estimate the variable of the ultra-local model and feed back it to the controller. The controller is used to control speed and current. The MFNTSMC method can be used to design the d-q-axis current controllers and speed controller for PMSM vector control system.

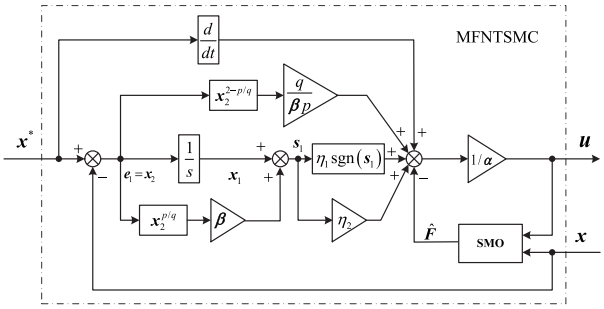

FIGURE 2. Schematic diagram of MFNTSMC.

A. DESIGN OF MFNTSMC CONTROLLER

The state error of the controller is designed as follows:

$$\boldsymbol{e}_1 = \boldsymbol{x}^* - \boldsymbol{x}, \tag{14}$$

where $\boldsymbol{e}_1 = \begin{bmatrix} e_{d1} & e_{q1} & e_{\omega 1} \end{bmatrix}^T$, and $e_{d1} = i_d^* - i_d$, $e_{q1} = i_q^* - i_q$, $e_{\omega 1} = \omega_e^* - \omega_e$. $\boldsymbol{x}^* = \begin{bmatrix} i_d^* & i_q^* & \omega_e^* \end{bmatrix}^T$, and i_d^*, i_q^* are the given value of d-q-axis current, ω_e^* is the given value of the rotor electrical angular velocity.

The state variables $\boldsymbol{x}_1 = \int \boldsymbol{e}_1$ and $\boldsymbol{x}_2 = \boldsymbol{e}_1$ are introducing, the state-space equation is as follows:

$$\begin{cases} \dot{\boldsymbol{x}}_1 = \boldsymbol{x}_2 \\ \dot{\boldsymbol{x}}_2 = \dot{\boldsymbol{x}}^* - \boldsymbol{\alpha}\boldsymbol{u} - \boldsymbol{F}. \end{cases} \tag{15}$$

A second-order nonsingular terminal sliding mode (NTSM) manifold is designed as follows [23]:

$$\boldsymbol{s}_1 = \boldsymbol{x}_1 + \boldsymbol{\beta}\boldsymbol{x}_2^{p/q}, \tag{16}$$

where $\boldsymbol{\beta} = diag\,(\beta_1, \beta_2, \beta_3)$, $\beta_1 > 0$, $\beta_2 > 0$, $\beta_3 > 0$ are the designed parameter; p, q are all odd, $1 < p/q < 2$.

Differentiating (16), the following equation is obtained:

$$\begin{aligned} \dot{\boldsymbol{s}}_1 &= \dot{\boldsymbol{x}}_1 + \boldsymbol{\beta}\frac{p}{q}\boldsymbol{x}_2^{p/q-1}\dot{\boldsymbol{x}}_2 \\ &= \boldsymbol{x_2} + \boldsymbol{\beta}\frac{p}{q}\boldsymbol{x}_2^{p/q-1}(\dot{\boldsymbol{x}}^* - \boldsymbol{F} - \boldsymbol{\alpha}\boldsymbol{u}). \end{aligned} \tag{17}$$

Theorem 1: For (15), the state error can converge to zero in finite time, if the NTSM manifold is chosen as equation (16) and the control law (18) is designed as follows:

$$\boldsymbol{u} = \frac{1}{\boldsymbol{\alpha}}[-\hat{\boldsymbol{F}} + \dot{\boldsymbol{x}}^* + \frac{1}{\boldsymbol{\beta}}\frac{q}{p}\boldsymbol{x}_2^{2-p/q} + \eta_1 sgn(\boldsymbol{s}_1) + \eta_2 \boldsymbol{s}_1], \tag{18}$$

where $\hat{\boldsymbol{F}}$ is the estimated values of $\boldsymbol{F}$; $\eta_1 > 0$, $\eta_2 > 0$ are the designed parameter; $\eta_1 \geq \left\| \hat{\boldsymbol{F}} - \boldsymbol{F} \right\| + \mu(\mu > 0)$.

Proof: The following Lyapunov function is selected to be:

$$V_1 = \frac{1}{2}\boldsymbol{s}_1^T\boldsymbol{s}_1. \tag{19}$$

Differentiating V_1 with respect to time, and substituting (17) into it, then the following equation is obtained:

$$\begin{aligned} \dot{V}_1 &= \boldsymbol{s}_1^T\dot{\boldsymbol{s}}_1 \\ &= \boldsymbol{s}_1^T\boldsymbol{\beta}\frac{p}{q}\boldsymbol{x}_2^{p/q-1}(\hat{\boldsymbol{F}} - \boldsymbol{F} - \eta_1 sgn(\boldsymbol{s}_1) - \eta_2\boldsymbol{s}_1) \\ &= \boldsymbol{s}_1^T\boldsymbol{\beta}\frac{p}{q}\boldsymbol{x}_2^{p/q-1}(\tilde{\boldsymbol{F}} - \eta_1 sgn(\boldsymbol{s}_1) - \eta_2\boldsymbol{s}_1) \\ &\leq \boldsymbol{\beta}\frac{p}{q}\boldsymbol{x}_2^{p/q-1}((\left\| \tilde{\boldsymbol{F}} \right\| - \eta_1)\left\| \boldsymbol{s}_1 \right\| - \eta_2\left\| \boldsymbol{s}_1 \right\|^2), \end{aligned} \tag{20}$$

where $\tilde{\boldsymbol{F}} = \hat{\boldsymbol{F}} - \boldsymbol{F}$ is bounded.

Because of $1 < p/q < 2$, $0 < p/q - 1 < 1$, and $p, q\,(p > q)$ are all odd, we got $\boldsymbol{x}_2^{p/q-1} > 0$; when $\eta_1 \geq \left\| \tilde{\boldsymbol{F}} \right\| + \mu(\mu > 0)$, then the following equation is obtained:

$$\dot{V}_1 \leq \boldsymbol{\beta}\frac{p}{q}\boldsymbol{x}_2^{p/q-1}(-\mu\left\| \boldsymbol{s}_1 \right\| - \eta_2\left\| \boldsymbol{s}_1 \right\|^2) \leq 0. \tag{21}$$

This completes the proof. □

The speed controller and the d-q-axis current controllers are designed by the proposed MFNTSMC. The structural diagram of the PMSM driven system is presented in Figure 3.

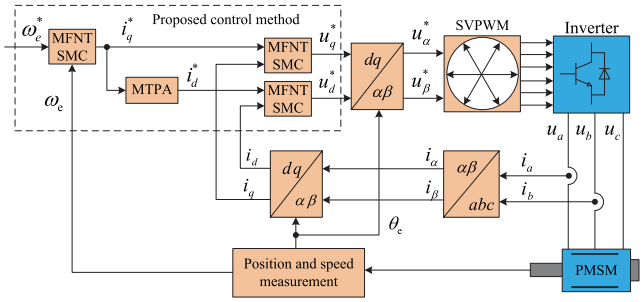

FIGURE 3. Schematic diagram of PMSM control system.

B. DESIGN OF SLIDING MODE OBSERVER

In equation (13), $\boldsymbol{F}$ is an unknown term, the sliding mode observer is designed to obtain the estimated value $\hat{\boldsymbol{F}}$. The sliding mode observer can be designed as follows:

$$\dot{\hat{\boldsymbol{x}}} = \boldsymbol{\alpha}\boldsymbol{u} + \boldsymbol{k}sgn(\boldsymbol{x} - \hat{\boldsymbol{x}}), \tag{22}$$

where $\boldsymbol{k} = diag\,(k_1, k_2, k_3)$; $k_1 > 0$, $k_2 > 0$, $k_3 > 0$ are all the designed parameter.

The observer error is defined as follows:

$$\boldsymbol{e}_2 = \boldsymbol{x} - \hat{\boldsymbol{x}}, \tag{23}$$

where $\boldsymbol{e}_2 = \begin{bmatrix} e_{d2} & e_{q2} & e_{\omega 2} \end{bmatrix}^T$, $\hat{\boldsymbol{x}} = \begin{bmatrix} \hat{i}_d & \hat{i}_q & \hat{\omega}_e \end{bmatrix}^T$. " ^ " denotes the estimated values, $e_{d2} = i_d - \hat{i}_d$, $e_{q2} = i_q - \hat{i}_q$, $e_{\omega 2} = \omega_e - \hat{\omega}_e$.

Then, the stator error equation can be obtained by subtracting (13) from (22):

$$\dot{\boldsymbol{e}}_2 = \boldsymbol{F} - \boldsymbol{k}sgn(\boldsymbol{e}_2). \tag{24}$$

Theorem 2: Choosing the sliding mode manifold $\boldsymbol{s}_2 = \boldsymbol{e}_2$, the stator error equation (24) will converge to zero in finite time if the appropriate $\boldsymbol{k}$ is chosen.

Proof: The following Lyapunov function is selected to be:

$$V_2 = \frac{1}{2}\boldsymbol{s}_2^T\boldsymbol{s}_2. \tag{25}$$

Differentiating (25) with respect to time, then the following equation is obtained:

$$\begin{aligned}\dot{V}_2 &= \boldsymbol{s}_2^T \dot{\boldsymbol{s}}_2 = \boldsymbol{e}_2^T \dot{\boldsymbol{e}}_2 \\ &= \boldsymbol{e}_2^T (\boldsymbol{F} - \boldsymbol{k} sgn(\boldsymbol{e}_2)) \\ &= \boldsymbol{e}_2^T \boldsymbol{F} - \boldsymbol{e}_2^T \boldsymbol{k} sgn(\boldsymbol{e}_2) \\ &\leq \|\boldsymbol{e}_2\| \|\boldsymbol{F}\| - k_1 |e_{d2}| - k_2 \left|e_{q2}\right| - k_3 |e_{\omega 2}| \\ &\leq \|\boldsymbol{e}_2\| (\|\boldsymbol{F}\| - k_4), \end{aligned} \tag{26}$$

where $k_4 = \min\{k_1, k_2, k_3\}$.

When $k_4 > \|\boldsymbol{F}\| + \eta$ ($\eta > 0$) is chosen, according to equation (26), the following equation is obtained:

$$\dot{V}_2 \leq -\eta \|\boldsymbol{e}_2\|. \tag{27}$$

Therefore, according to the Lyapunov stability criterion and the sliding mode reachability condition, the stator error $\boldsymbol{e}_2$ will converge to zero in finite time, and it can be known that observer is asymptotically stable.

This completes the proof. □

Remark 2: When stator error stays on the sliding mode manifold, it satisfies $\boldsymbol{e}_2 = \dot{\boldsymbol{e}}_2 = 0$, according to the sliding mode equivalent control method [24], the following equation is obtained by equation (24):

$$\hat{\boldsymbol{F}} = \boldsymbol{k} sgn(\boldsymbol{e}_2). \tag{28}$$

IV. SIMULATION RESULTS

In order to verify the effectiveness of the proposed MFNTSMC method, the Matlab/Simulink is used to simulate PMSM driven system. The vector control scheme of Maximum Torque Per Ampere (MTPA) is adopted. The sampling period T_s is set as $5 \cdot 10^{-6}$ s. The PMSM parameters are listed in Table 1.

TABLE 1. Nominal parameters of permanent magnet synchronous motor.

Parameters	Unit	Values
Rated voltage (U_N)	V	1500
Stator resistance (R_s)	Ω	0.02
Number of pole pairs (n_p)	paires	4
q-axis inductance (L_q)	H	0.003572
d-axis inductance (L_d)	H	0.001500
Rotor PM flux (ψ_{ro})	Wb	0.892
Rotational Inertia (J)	$kg \cdot m^2$	100
Viscous friction coefficient (B)	$Nm \cdot s/rad$	0.001

A. SIMULATION FOR PMSM IN NORMAL CONDITIONS

The simulation time is set as 6 s. The initial rotor electrical angular velocity is set to 50 rad/s and subsequently increases to 200 rad/s at 2 s; The initial load torque is set to 1000 Nm and subsequently increases to 3000 Nm at 4 s. The simulation results are shown in Figure 4-Figure 13.

Figure 4 demonstrates the speed comparison diagram by the proposed MFNTSMC method, MFC method and PI method. When the speed increases at 2 s, the speed response of the motor controlled by MFNTSMC method is faster than PI method, and compared with MFC method, the error

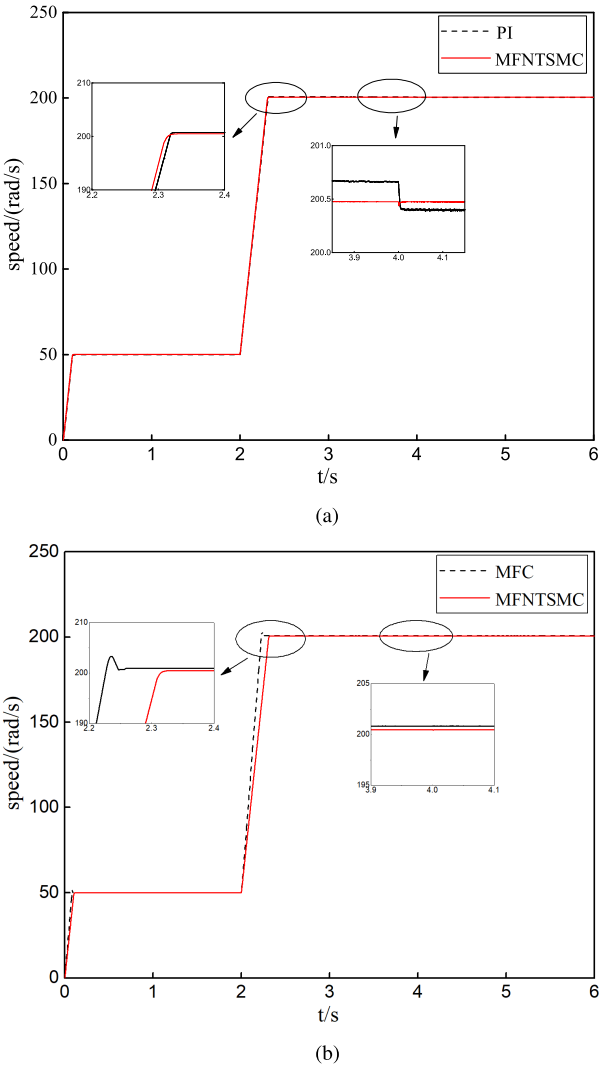

FIGURE 4. Comparison diagram of speed. (a) PI and MFNTSMC. (b) MFC and MFNTSMC.

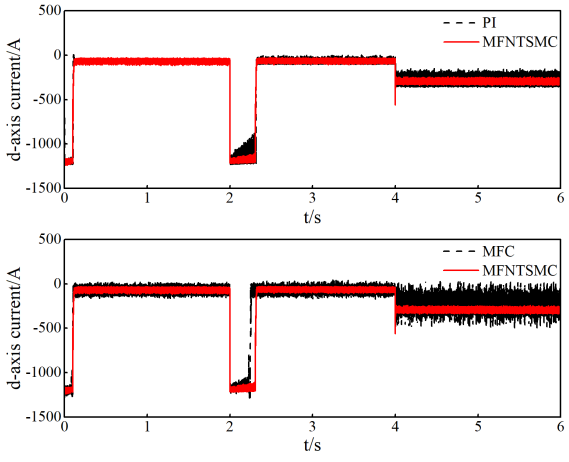

FIGURE 5. Comparison diagram of *d*-axis current.

is smaller. When the torque increased at 4 s, it can be seen from the enlargement diagram, the speed controlled by PI control method has a relatively obvious reduction process.

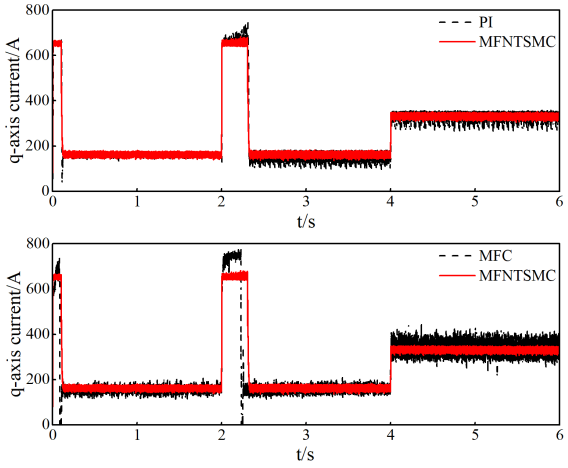

FIGURE 6. Comparison diagram of q-axis current.

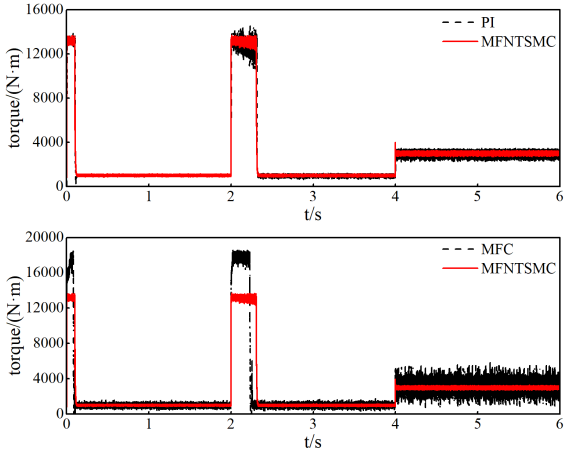

FIGURE 7. Comparison diagram of torque.

The speed controlled by MFNTSMC method is not obvious, and the steady-state error is small. Compared with MFC method, the speed error controlled by MFNTSMC method is smaller. Figure 5 and Figure 6 show the comparison diagram of d-q-axis current by the proposed MFNTSMC method, MFC method and PI method. It clearly shown that the d-q-axis current pulsation controlled by the MFNTSMC method is smaller than PI method and MFC method. The comparison diagram of torque controlled by proposed MFNTSMC method, MFC method and PI method are presents in Figure 7. It can be seen that the torque pulsation controlled by the MFNTSMC method is smaller than PI method.

Figure 8-Figure 13 demonstrate the results of sliding mode observer of MFNTSMC in normal condition. Figure 8-Figure 9 demonstrate the observed results of speed and the estimated value of F_ω. Figure 10-Figure 11 show the observed results of d-axis current and the estimated value of F_d. Figure 12-Figure 13 show the observed results of q-axis current and the estimated value of F_q. It is known that the

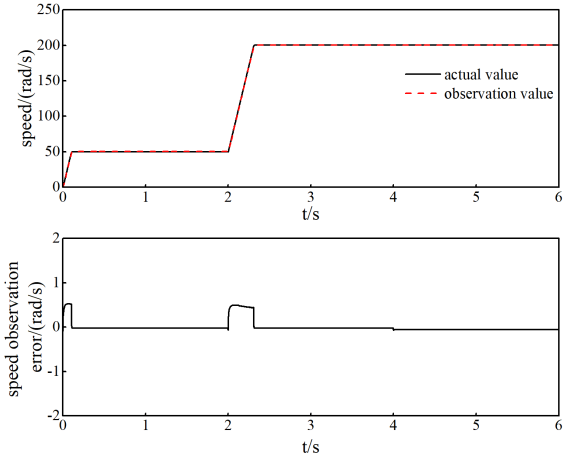

FIGURE 8. The observation results of speed.

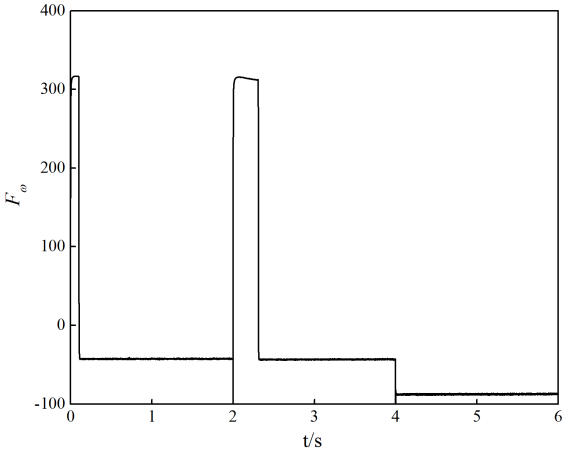

FIGURE 9. The estimated value of F_ω.

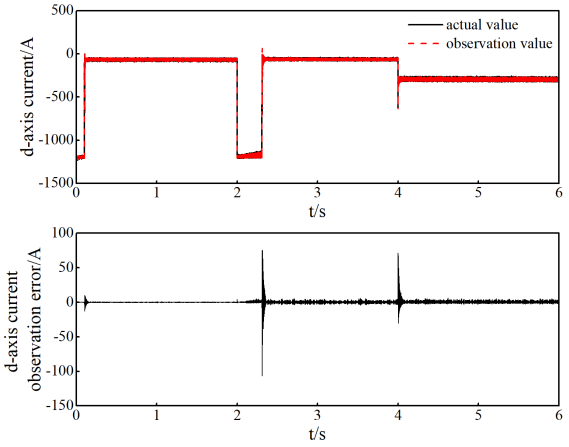

FIGURE 10. The observation results of d-axis current.

estimated error of speed and d-q-axis current are small. When some variables have been changed, the error will change, and it will converge to zero in short time.

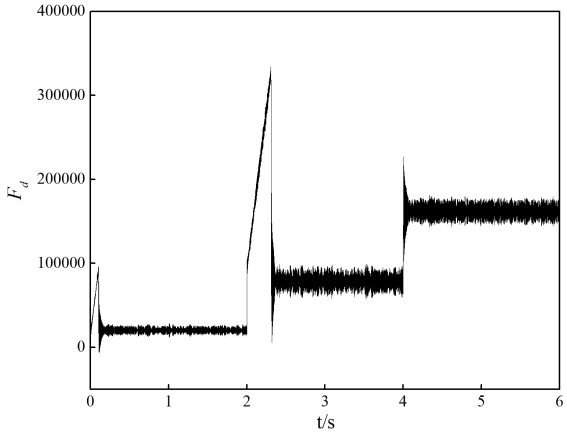

FIGURE 11. The estimated value of F_d.

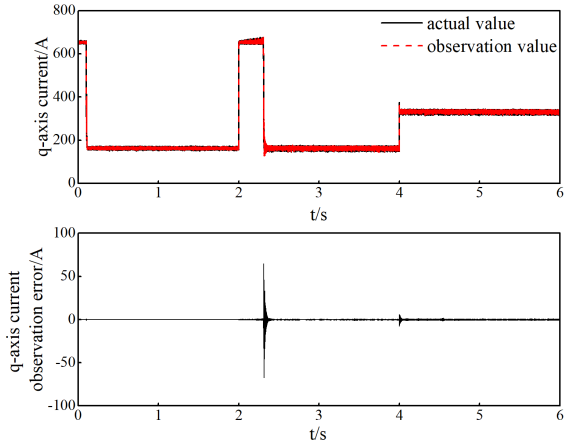

FIGURE 12. The observation results of q-axis current.

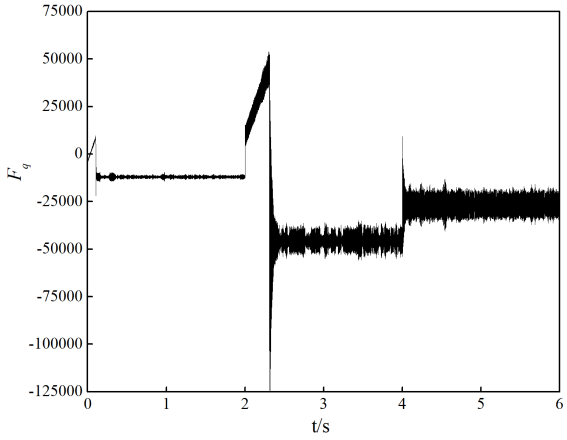

FIGURE 13. The estimated value of F_q.

It can be drawn from the simulation result that the motor speed controlled by MFNTSMC is faster than PI, and the robustness is better than PI method and MFC method.

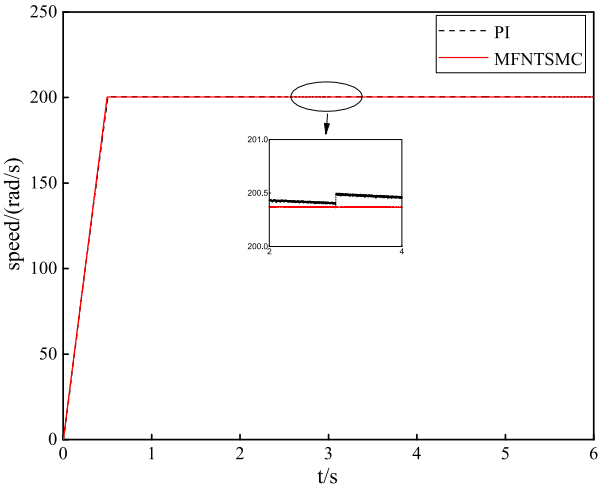

(a)

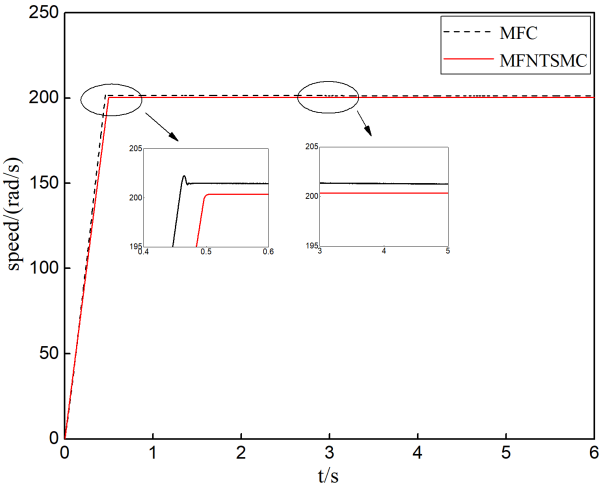

(b)

FIGURE 14. Comparison diagram of speed. (a) PI and MFNTSMC. (b) MFC and MFNTSMC.

B. SIMULATION FOR PMSM IN PM DEMAGNETIZATION

The simulation time is set as 6 s, the given speed is 200 rad/s, and the given torque is 3000 Nm. The PM demagnetization occurs at 3 s, the flux linkage amplitude is set to 0.4 Wb, and the flux linkage deviation angle is set to 0 to $\pi/4$. The simulation results are shown in Figures 14-Figures 23 by the proposed MFNTSMC method, MFC method and PI control method.

The comparison diagram of speed is shown in Figure 14. When PM demagnetization occurs at 3 s, the speed controlled by MFNSMC method and MFC method can still keep up with the given value, but the speed error of MFNTSMC method is smaller. It can be seen from Figure 15 and Figure 16, when the PM demagnetization occurs at 3 s, the d-q-axis currents change quickly. Compared with the PI control method and MFC method, the current controlled by MFNTSMC method is restored to stability in short time, and the current

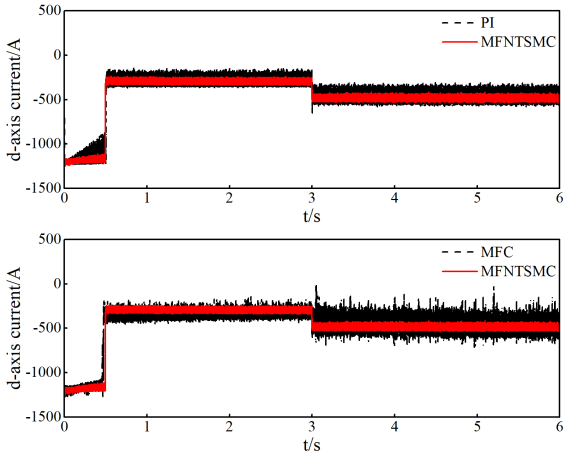

FIGURE 15. Comparison diagram of *d*-axis current.

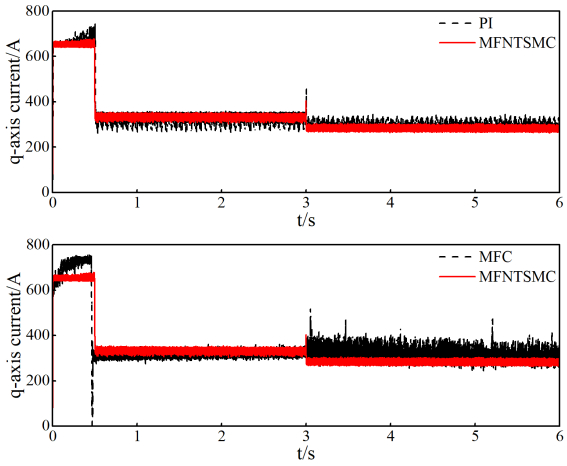

FIGURE 16. Comparison diagram of *q*-axis current.

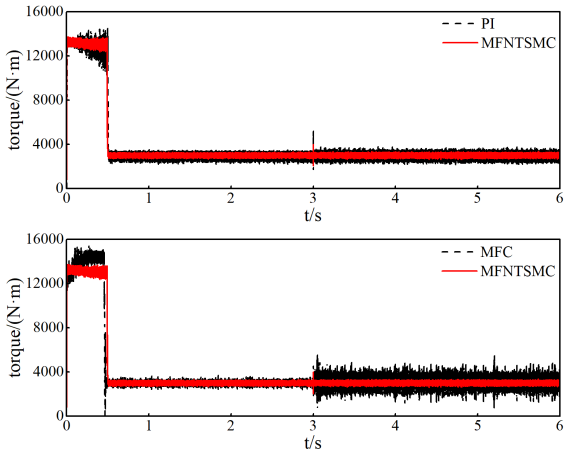

FIGURE 17. Comparison diagram of torque.

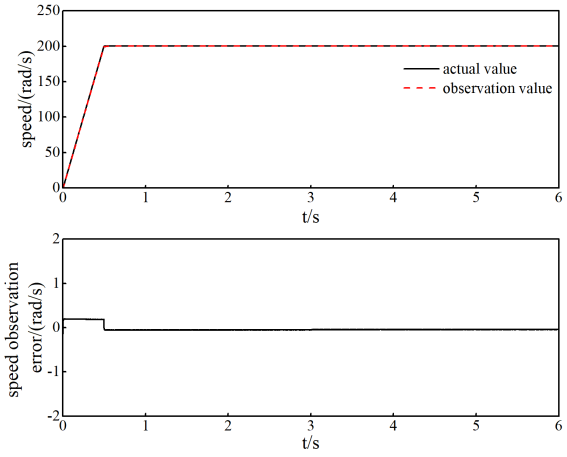

FIGURE 18. The observation results of speed.

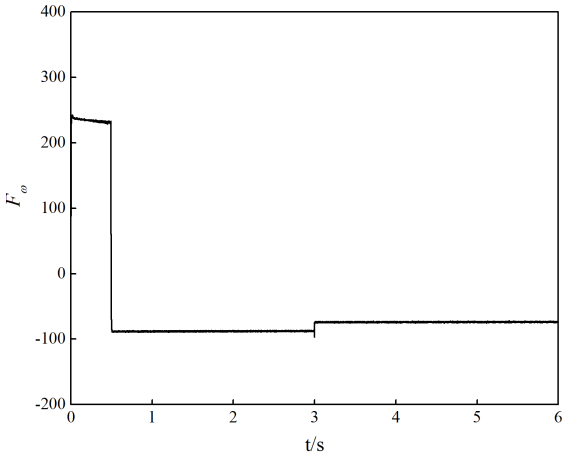

FIGURE 19. The estimated value of F_ω.

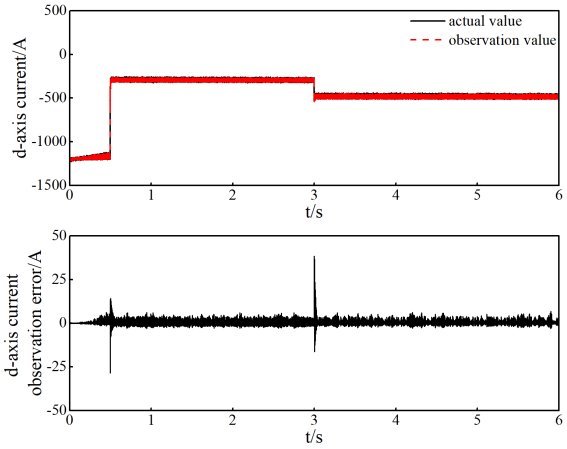

FIGURE 20. The observation results of *d*-axis current.

pulsation is relatively small. Figure 17 shows that the torque will fluctuate when the PM demagnetization occurs at 3 s. But the torque will restored to a stable value quickly.

Figure 18-Figure 23 demonstrate the results of sliding mode observer of MFNTSMC in PM demagnetization. Figure 18-Figure 19 show the observed results of speed and the estimated value of F_ω Figure 20-Figure 21 show that the

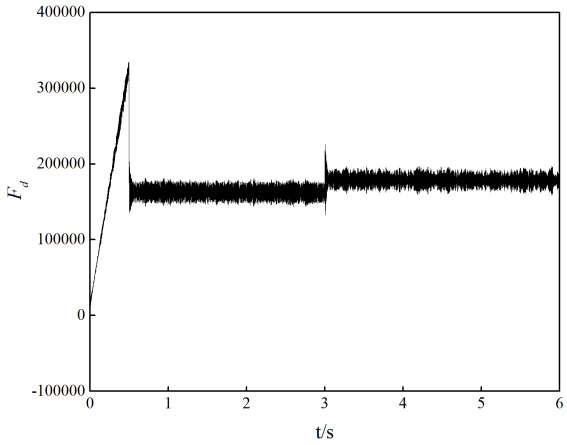

FIGURE 21. The estimated value of F_d.

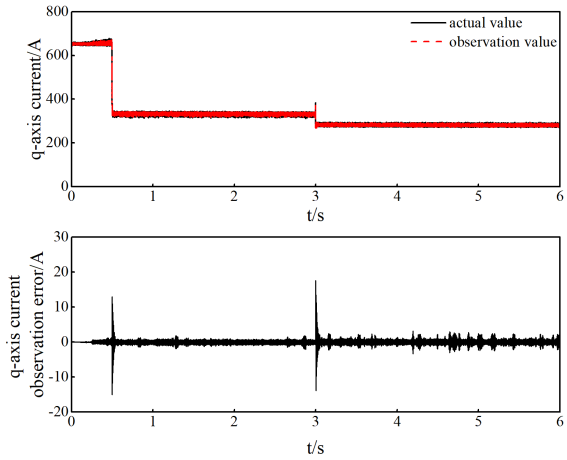

FIGURE 22. The observation results of q-axis current.

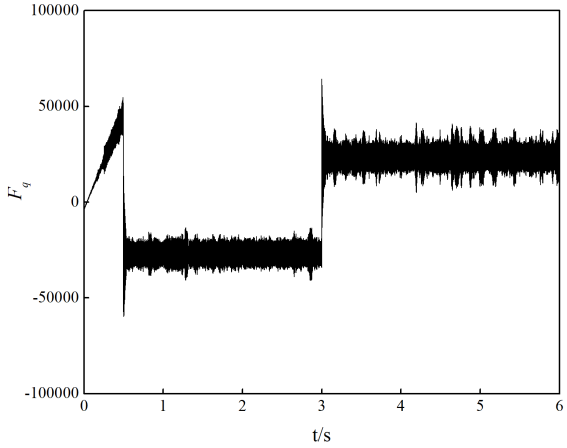

FIGURE 23. The estimated value of F_q.

observed results of d-axis current and the estimated value of F_d. And the observed results of q-axis current and the estimated value of F_q are shown in Figure 22-Figure 23. It is known that the estimated error of speed and current is small.

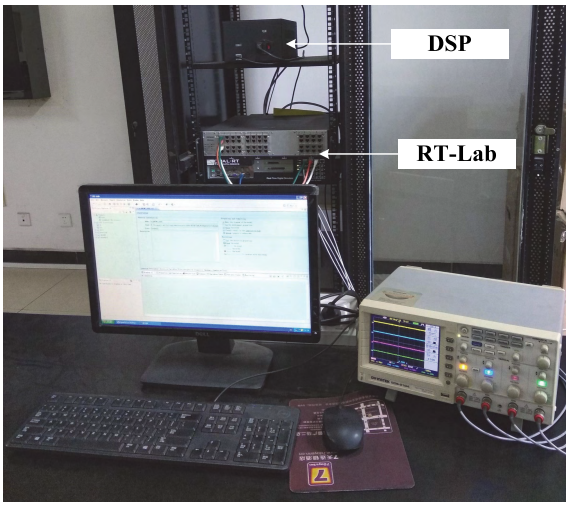

FIGURE 24. The RT-Lab HILS platform.

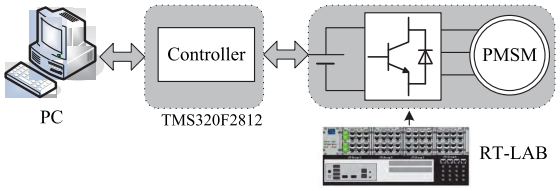

FIGURE 25. Configuration of the RT-Lab HILS system.

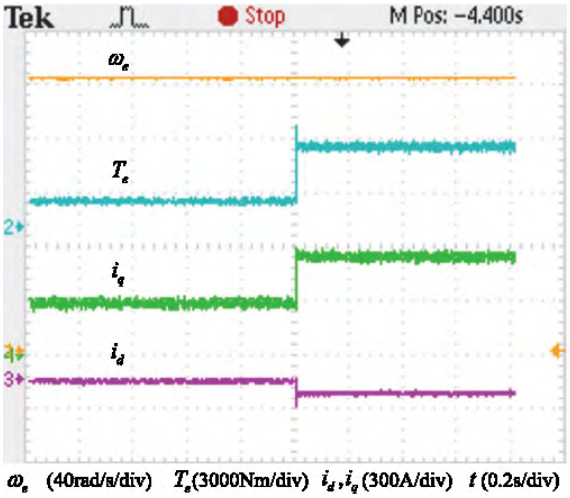

FIGURE 26. The experimental result of MFNTSMC method in normal condition.

When the PM demagnetization occurs, the error will change, and it will converge to zero in short time.

Compared with PI control method and MFC method, the steady-state error controlled by MFNTSMC method is smaller. It is known that the MFNTSMC algorithm has strong robustness when the permanent magnet has a demagnetization fault.

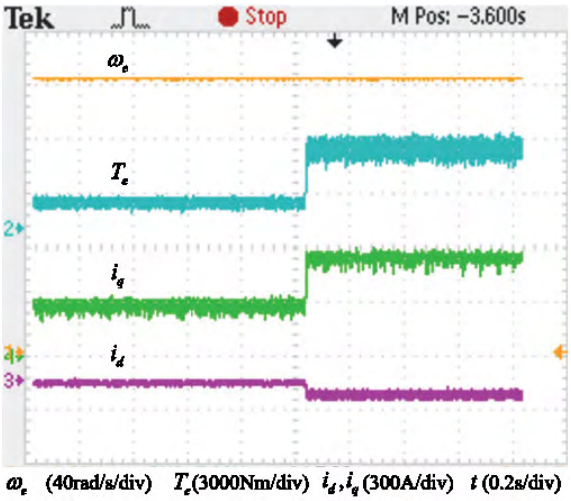

FIGURE 27. The experimental result of PI control method in normal condition.

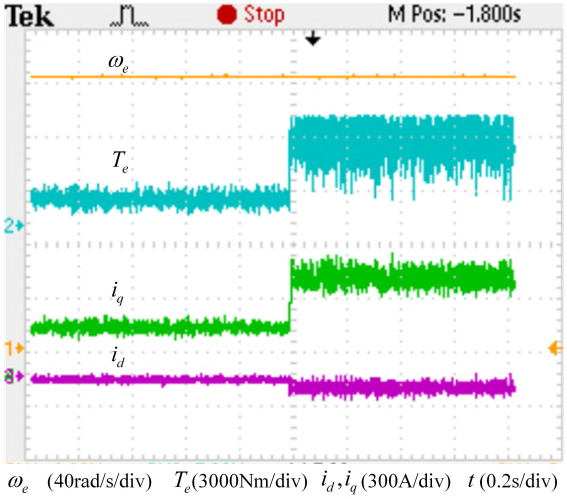

FIGURE 28. The experimental result of MFC control method in normal condition.

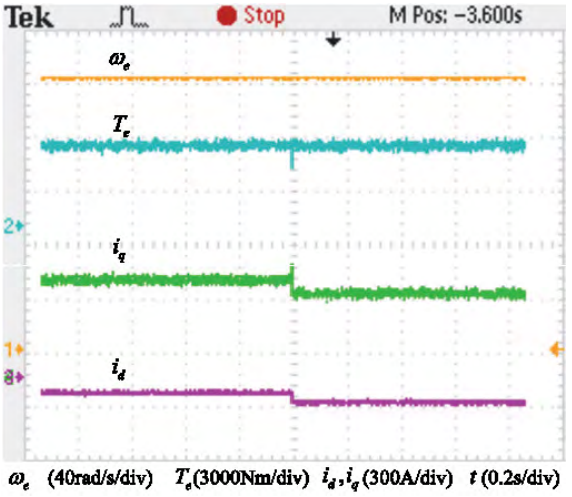

FIGURE 29. The experimental result of MFNTSMC method in PM demagnetization.

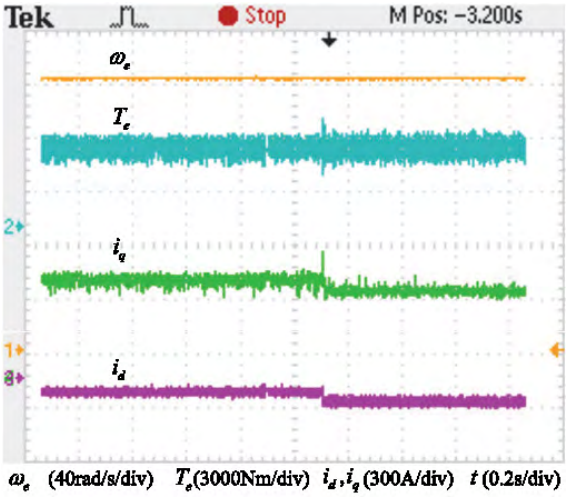

FIGURE 30. The experimental result of PI control method in PM demagnetization.

V. EXPERIMENT RESULTS

PM demagnetization is difficult to simulate. Thus, the RT-Lab hardware-in-the-loop simulation (HILS) platform is used in this work. The RT-Lab HILS platform is composed of DSP controller, OP5600 simulation motor, and upper computer monitoring interface, etc. The RT-Lab HILS platform is shown in Figure 24, and the configuration of the RT-Lab hardware-in-the loop simulation system is shown in Figure 25 [20]. The experimental results are shown in Figures 26-31. The sampling period T_s is set as $5 \cdot 10^{-6}$ s.

A. PERFORMANCE COMPARISON OF MFNTSMC, PI AND MFC IN PMSM NORMAL CONDITIONS

In Figure 26 to Figure 28, the experimental results of the rotor electrical angular velocity (ω_e), the torque (T_e), the d-q-axis current (i_d,i_q) controlled by the MFNTSMC method, PI control method and MFC method in normal condition are shown. As show in Figure 26 to Figure 28, the pulsation controlled by MFNTSMC method is smaller than PI control method and MFC method.

B. PERFORMANCE COMPARISON OF MFNTSMC, PI AND MFC IN PM DEMAGNETIZATION

Figure 29 to Figure 31 show the experimental results of the rotor electrical angular velocity (ω_e), the torque (T_e), the d-q-axis current (i_d, i_q) controlled by the MFNTSMC method, PI control method and MFC method under PM demagnetization. The results show that the motor torque and current pulsation controlled by MFNTSMC method is small than PI method and MFC method. When the PM demagnetization occurs, the torque and current controlled by MFNTSMC method restored to a stable value in short time.

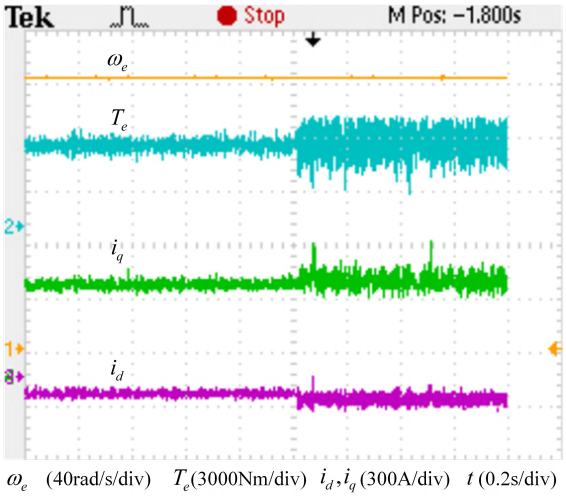

FIGURE 31. The experimental result of MFC control method in PM demagnetization.

It is proved that the MFNTSMC method has strong robustness and has fault-tolerant control functions for PM demagnetization.

VI. CONCLUSION

The novel MFNTSMC algorithm for PMSM drives system is proposed in this paper. The ultra-local model is constructed based on the input and output of the PMSM system. The speed and *d*-*q*-axis current controllers are designed by MFNTSMC, and the SMOs are designed to estimate the unknown variables in the ultra-local model. Compared with the PI control method and MFC method, the results of simulations and experimentations verify the efficiency of the proposed MFNTSMC scheme. The MFNTSMC method can increase the response speed and robustness in normal condition, and has fault-tolerant control function for PM demagnetization fault. When the PM demagnetization occurs, the simulations and experimentations indicate that the MFNTSMC method can operates well. The MFNTSMC controller can reduce the dependence on the precise model of PMSM system, and increase the response speed and robustness.

REFERENCES

[1] K. Zhao, P. Li, C. Zhang, X. Li, J. He, and Y. Lin, "Sliding mode observer-based current sensor fault reconstruction and unknown load disturbance estimation for PMSM driven system," *Sensors*, vol. 17, no. 12, p. E2833, Dec. 2017.

[2] C. Zhang, G. Wu, J. He, J. Feng, and K. Zhao, "Fault-tolerant predictive control for demagnetization faults in permanent magnet synchronous machine," *Trans. China Electrotech. Soc.*, vol. 32, no. 15, pp. 100–110, Aug. 2017.

[3] H. Li, T. Chen, and H. Yao, "Mechanism, diagnosis and development of demagnetization fault for pmsm in electric vehicle," *Trans. China Electrotech. Soc.*, vol. 28, no. 8, pp. 276–284, Aug. 2013.

[4] H. Li and T. Chen, "Demagnetization fault diagnosis and fault mode recognition of pmsm for EV," *Trans. China Electrotech. Soc.*, vol. 32, no. 5, pp. 1–8, Mar. 2017.

[5] X. Liu, H. Yu, J. Yu, and L. Zhao, "Combined speed and current terminal sliding mode control with nonlinear disturbance observer for PMSM drive," *IEEE Access*, vol. 6, pp. 29594–29601, 2018.

[6] C. Zhang *et al.*, "Robust fault-tolerant predictive current control for permanent magnet synchronous motors considering demagnetization fault," *IEEE Trans. Ind. Electron.*, vol. 65, no. 7, pp. 5324–5334, Jul. 2018.

[7] C. Zhang, G. Wu, J. He, and K. Zhao, "Sliding observer-based demagnetisation fault-tolerant control in permanent magnet synchronous motors," *J. Eng.*, vol. 2017, no. 6, pp. 175–183, Jun. 2017.

[8] Y. Al Younes, A. Drak, H. Noura, A. Rabhi, and A. El Hajjaji, "Robust model-free control applied to a quadrotor UAV," *J. Intell. Robot. Syst.*, vol. 84, nos. 1–4, pp. 37–52, Dec. 2016.

[9] M. Doublet, C. Join, and F. Hamelin, "Model-free control for unknown delayed systems," in *Proc. 3rd Conf. Control Fault-Tolerant Syst. (SysTol)*, R. Sarrate, Ed. Barcelone, Spain: IEEE Press, Sep. 2016, pp. 630–635.

[10] M. Fliess and C. Join, "Model-free control," *Int. J. Control*, vol. 86, no. 12, pp. 2228–2252, May 2013.

[11] A. Barkat, B. Marinescu, C. Join, and M. Fliess, "Model-free control for VSC-based HVDC systems," in *Proc. IEEE PES Innov. Smart Grid Technol. Conf. Eur. (ISGT-Europe)*, Sarajevo, Bosnia-Herzegovina, Oct. 2018, pp. 1–6.

[12] D. Tognin, M. Rampazzo, M. Pagan, L. Carniello, and A. Beghi, "Model-free control of an artificial tide generation experimental apparatus," *IFAC-PapersOnLine*, vol. 51, no. 4, pp. 829–834, Jan. 2018.

[13] H. Thabet, M. Ayadi, and F. Rotella, "Experimental comparison of new adaptive PI controllers based on the ultra-local model parameter identification," *Int. J. Control, Automat. Syst.*, vol. 14, no. 6, pp. 1520–1527, Dec. 2016.

[14] H. Ahmed, I. Salgado, and H. Ríos, "Robust synchronization of master-slave chaotic systems using approximate model: An experimental study," *ISA Trans.*, vol. 73, pp. 141–146, Feb. 2018.

[15] Y. Zhou, H. Li, and H. Yao, "Model-free control of surface mounted PMSM drive system," in *Proc. IEEE Int. Conf. Ind. Technol. (ICIT)*, Taipei, Taiwan, Mar. 2016, pp. 175–180.

[16] Y. Zhou, H. Li, and H. Zhang, "Model-free deadbeat predictive current control of a surface-mounted permanent magnet synchronous motor drive system," *J. Power Electron.*, vol. 18, no. 1, pp. 103–115, Jan. 2018.

[17] Y. A. Younes, A. Drak, H. Noura, A. Rabhi, and A. El Hajjaji, "Model-free control of a quadrotor vehicle," in *Proc. Int. Conf. Unmanned Aircr. Syst. (ICUAS)*. Orlando, FL, USA, May 014, pp. 1126–1131.

[18] K. Zhao, T. Chen, C. Zhang, J. He, and G. Huang, "Sensorless and torque control of IPMSM applying NFTSMO," *Chin. J. Sci. Instrum.*, vol. 36, no. 2, pp. 294–303, Feb. 2015.

[19] I. Boldea, M. C. Paicu, and G. D. Andreescu, "Active flux concept for motion-sensorless unified AC drives," *IEEE Trans. Power Electron.*, vol. 23, no. 5, pp. 2612–2618, Sep. 2008.

[20] K.-H. Zhao *et al.*, "Accurate torque-sensorless control approach for interior permanent-magnet synchronous machine based on cascaded sliding mode observer," *J. Eng.*, vol. 2017, no. 7, pp. 376–384, Jun. 2017.

[21] A. Andersson and T. Thiringer, "Motion sensorless IPMSM control using linear moving horizon estimation with luenberger observer state feedback," *IEEE Trans. Transport. Electrific.*, vol. 4, no. 2, pp. 464–473, Jun. 2018.

[22] K.-H. Zhao, T.-F. Chen, C.-F. Zhang, J. He, and G. Huang, "Online fault detection of permanent magnet demagnetization for IPMSMS by nonsingular fast terminal-sliding-mode observer," *Sensors*, vol. 14, no. 12, pp. 23119–23136, Dec. 2014.

[23] Y. Feng, X. Yu, and Z. Man, "Non-singular terminal sliding mode control of rigid manipulators," *Automatica*, vol. 38, no. 12, pp. 2159–2167, Dec. 2002.

[24] S. K. Spurgeon, "Sliding mode observers: A survey," *Int. J. Syst. Sci.*, vol. 39, no. 8, pp. 751–764, Aug. 2008.

KAIHUI ZHAO received the B.S. degree in electric traction and transmission control from the Changsha Railway Institute, Changsha, China, in 1997, the M.S. degree in computer application technology from Southeast University, Nanjing, China, in 2005, and the Ph.D. degree in traffic information engineering and control from Central South University, Changsha, in 2015.

Since 2005, he has been with the College of Electrical and Information Engineering, Hunan University of Technology, Zhuzhou, where he has been an Associate Professor, since 2007. His research interests include fault diagnosis on electric machines and industrial process control.

TONGHUAN YIN received the B.S. degree from the Wuchang University of Technology, Wuhan, China, in 2016. He is currently pursuing the M.S. degree with the College of Electrical and Information Engineering, Hunan University of Technology, Zhuzhou, China.

His research interests include electric traction and transmission control.

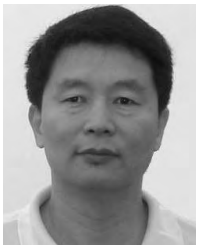

CHANGFAN ZHANG received the M.S. degree in electronics engineering from Southwest Jiaotong University, Chengdu, China, in 1989, and the Ph.D. degree in control theory and engineering from Hunan University, Changsha, China, in 2001. He was a Postdoctoral Fellow with Central South University, Changsha, from 2001 to 2003, and a Visiting Scholar with the University of Waterloo, Waterloo, Canada, from 2007 to 2008.

He is currently a Professor with the College of Electrical and Information Engineering, Hunan University of Technology. His research interests include fault diagnosis on electric machines and industrial process control.

JING HE received the M.S. degree in computer engineering from the Central South University of Forestry and Technology, Changsha, China, in 2002, and the Ph.D. degree in mechatronics engineering from the National University of Defense Technology, Changsha, in 2009. She was a Visiting Scholar with the Helsinki University of Technology, Helsinki, Finland, from 2004 to 2005, and also with the University of Waterloo, Waterloo, Canada, from 2007 to 2008. Since 2011, she has been a Postdoctoral Fellow with the National University of Defense Technology.

She is currently a Professor with the College of Electrical and Information Engineering, Hunan University of Technology. Her research interests include fault diagnosis on mechatronics and industrial process control.

XIANGFEI LI received the M.S. degree from Zhengzhou University, Zhengzhou, China, in 1999, and the Ph.D. degree in control theory and control engineering from Central South University, Changsha, China, in 2003.

He is currently a Professor with the College of Electrical and Information Engineering, Hunan University of Technology, Zhuzhou. His present research interests include electric traction and transmission control.

YUE CHEN received the B.S. degree from Fuyang Normal University, Fuyang, China, in 2017. He is currently pursuing the M.S. degree with the College of Electrical and Information Engineering, Hunan University of Technology, Zhuzhou, China.

His research interests include fault diagnosis and nonlinear control of permanent magnet synchronous motor.

RUIRUI ZHOU received the B.S. degree from the Heilongjiang University of Science and Technology, Harbin, China, in 2018. He is currently pursuing the M.S. degree with the College of Electrical and Information Engineering, Hunan University of Technology, Zhuzhou, China.

His research interests include fault diagnosis and fault-tolerant control of permanent magnet synchronous motor.

AOJIE LENG received the B.S. degree from Fuyang Normal University, Fuyang, China, in 2017. He is currently pursuing the M.S. degree with the College of Electrical and Information Engineering, Hunan University of Technology, Zhuzhou, China.

His research interests include fault diagnosis and nonlinear control of permanent magnet synchronous motor.